

# TECHNICAL RESEARCH REPORT

## A Global Basis Function Approach to DC Glow Discharge Simulation

*by Y-H Lin, R. Adomaitis*

**T.R. 97-81**



*Sponsored by  
the National Science Foundation  
Engineering Research Center Program,  
the University of Maryland,  
Harvard University,  
and Industry*

# A Global Basis Function Approach to DC Glow Discharge Simulation

Yi-hung Lin and Raymond A. Adomaitis\*

*Department of Chemical Engineering and*

*Institute for Systems Research*

*University of Maryland*

*College Park, MD 20742*

## Abstract

A global discretization approach was taken to solve a self-consistent DC glow discharge model to study the interplay between modeling assumptions and convergence of the numerical solution techniques. It was found that the assumed form of electron diffusivity temperature dependence had a profound influence on the computed solutions. The numerical techniques developed offer a simple to implement alternative for plasma model discretization.

keywords: Collocation; Continuation; Global basis functions; Glow discharge; Plasma processing; Pseudospectral

## 1 Introduction

Plasmas with low gas pressure ( $1\text{mtorr}$  to  $10\text{torr}$ ), temperature (300 to  $500\text{K}$ ), and degree of ionization ( $10^{-6}$  to  $10^{-1}$ ) are used extensively for manufacturing integrated circuits (ICs). Plasma processing is a key fabrication step, especially for etching and deposition of thin films. Despite the wide use of the processes, there are virtually no commercial computer-aided design tools for plasma processing reactors based on first-principles models. Even though three-dimensional simulation tools are emerging [1], the computational cost is still unaffordable to most users since these simulators require supercomputer-sized computational resources. One primary reason is that current simulation techniques inevitably result in a finely-resolved spatial discretization mesh in the plasma sheath regions.

---

\*Phone: (301) 405-2969, Fax: (301) 314-9927, Email: adomaiti@isr.umd.edu

In this paper, we report on solutions to a fluid simulation for the plasma physics submodel<sup>1</sup> with a direct current (DC) ionization source by a pseudospectral (PS) discretization method. We present this global basis function approach as an alternative to localized basis function discretizations such as finite elements [4] and the block implicit implementation of finite differences [5]. Our approach is motivated by the excellent convergence property of the PS method [6], the transparency of its implementation to discretizing partial differential equations (PDEs) and their boundary conditions (BCs), and the great flexibility of selecting and optimizing trial functions for particular applications.

## 2 Modeling Equations

The smallest set of self-consistent continuum modeling equations consists of four partial differential equations and their associated boundary conditions: Poisson's equation, electron and ion continuity equations, and the electron energy balance. These equations can be solved for potential field, electron and ion number densities, and electron temperature. Electric field strengths, particle fluxes, and ionization rates may then be computed as secondary quantities from these solutions.

The model used in this report is similar to Graves and Jensen's [4]. The boundary conditions and parameters for the argon-like gas were also taken from [4]. One difference, however, is the expression for electron flux  $\vec{j}_e$  and the electron diffusivity  $D_e$ :

$$\begin{aligned}\vec{j}_e &= -D_e \vec{\nabla} n_e - \mu_e n_e \vec{E} \\ D_e &= \mu_e \frac{k_b T_e}{e}\end{aligned}\tag{1}$$

where  $n_e$ ,  $\mu_e$ , and  $T_e$  are electron number density, mobility, and temperature, respectively.  $\vec{E}$  is the electric field strength,  $k_b$  is the Boltzmann constant, and  $e$  is the unit charge. Our expression for temperature-dependent diffusivity implicitly assumes  $T_e \nabla n_e \gg n_e \nabla T_e$ , an assumption valid for the results presented in this paper. The dimensionless modeling equations for DC simulation are listed below in the order of Poisson, electron and ion continuity, and electron energy equations. While only one-dimensional discharge simulations are reported in this paper (so  $\nabla = \zeta \frac{\partial}{\partial Z}$  and  $\nabla^2 = \zeta^2 \frac{\partial^2}{\partial Z^2}$ ), the following nondimensional model is valid for higher dimensions and so is written in vector notation.

$$\begin{aligned}\nabla^2 \Phi &= -\epsilon(u_+ - u_e) \\ \vec{\nabla} \cdot \vec{J}_e &= k_2 u_e \\ \vec{\nabla} \cdot \vec{J}_+ &= k_2 u_e \\ \vec{\nabla} \cdot \vec{Q}_e &= \epsilon_e \vec{J}_e \cdot \vec{\nabla} \Phi - k_2 u_e\end{aligned}$$

---

<sup>1</sup>The fluid type formulation for the plasma physics submodels (for the detailed classification see [2]) have had great success in explaining the physics of the glow discharge [3]. The results are comparable to those by Monte Carlo particle simulation techniques.

The four basic variables are defined as  $\Phi = \frac{V}{V_0}$ ,  $u_e = \frac{n_e}{n_0}$ ,  $u_+ = \frac{n_+}{n_0}$ , and  $T = \frac{T_e}{T_{e0}}$ . The resultant auxiliary equations for electron, ion, and electron energy fluxes, and ionization rate coefficient are

$$\begin{aligned}\vec{J}_e &= -\frac{T}{D}\vec{\nabla}u_e + P_e u_e \vec{\nabla}\Phi \\ \vec{J}_+ &= -\left(\frac{1}{D_{e+}}\right)\vec{\nabla}u_+ - \left(\frac{P_+}{D_{e+}}\right)u_+ \vec{\nabla}\Phi \\ \vec{Q}_e &= \frac{5}{3H_i}\left(-\frac{T u_e}{D}\vec{\nabla}T + T\vec{J}_e\right) \\ k_2 &= D_a e^{-\frac{E}{T}}.\end{aligned}$$

The boundary conditions at  $z = 0$  (grounded electrode) are

$$\begin{aligned}\Phi &= 0 \\ u_e &= 0 \\ \nabla u_+ &= 0 \\ \frac{5}{3}\nabla T - \varepsilon_e H_i \nabla \Phi &= 0;\end{aligned}$$

and at  $z = 1$  (powered electrode)

$$\begin{aligned}\Phi &= -\Phi_{DC} \\ -\left(\frac{T}{D}\right)\nabla u_e + P_e u_e \nabla \Phi &= \left(\frac{\gamma P_+}{D_{e+}}\right)u_+ \nabla \Phi \\ \nabla u_+ &= 0 \\ T &= T_c.\end{aligned}$$

The values of nondimensional parameters are calculated in Table (1). The gas and scaling parameters used are listed in Table (2).

Symbol	Definition	Value	Symbol	Definition	Value
$\epsilon$	$\frac{\epsilon n_0 R^2}{\epsilon_0 V_0}$	406	$D_{e+}$	$\frac{D_e}{D_+}$	$10^4$
$D$	$10^6 / (\mu_e \frac{k_b T_{e0}}{e})$	5	$E$	$\frac{E_i}{k_b T_{e0}}$	24
$D_a$	$\frac{k_{i0} R^2 N}{D_e}$	$1.83 \times 10^6$	$\varepsilon_e$	$\frac{e V_0}{H_{ei}}$	29.5
$P_e$	$\frac{\mu_e V_0}{D_e}$	92	$H_i$	$\frac{H_{ei}}{\frac{3}{2} k_b T_{e0}}$	10.4
$P_+$	$\frac{\mu_+ V_0}{D_+}$	9200	$\zeta$	$\frac{R}{L}$	1.44

Table 1: Values of dimensionless parameters used in simulations

Symbol	Description	Value
$L$	interelectrode spacing	$3.525cm$
$R$	radius of the electrode	$5.08cm$
$N$	neutral density	$2.83 \times 10^{16}cm^{-3}$
$n_0$	reference density for charge particles	$4 \times 10^9cm^{-3}$
$V_0$	reference voltage	$460V$
$T_{e0}$	reference electron temperature	$1eV$
$D_+$	ion diffusivity	$10^2 \frac{cm^2}{sec}$
$\mu_e$	electron mobility	$2 \times 10^5 \frac{cm^2}{V \cdot sec}$
$\mu_+$	ion mobility	$2 \times 10^3 \frac{cm^2}{V \cdot sec}$
$E_i$	ionization rate activation energy	$24eV$
$H_{ei}$	ionization enthalpy loss	$15.578eV$
$\gamma$	secondary electron coefficient	$0.046$
$V_{DC}$	direct current voltage	$77.4V$
$k_{io}$	ionization rate prefactor	$2.5 \times 10^{-6} \frac{cm^3}{sec}$
$T_{ec}$	electron temperature at cathode	$0.5eV$

Table 2: Gas and Scaling Parameters

### 3 Numerical Methods

#### 3.1 Discretization

The modeling equations and boundary conditions are discretized and solved by a weighted residual method that combines elements of collocation and pseudospectral methods. If each of the states ( $\Phi$ ,  $u_e$ ,  $u_+$ , or  $T$ ) is represented by a linear combination of trial functions  $\psi_i(z)$  defined over  $0 \leq z \leq 1$ , i.e.,

$$u(z) = \sum_{i=1}^N c_i \psi_i(z),$$

a set of residual functions over  $z$  and at the boundaries can be defined with the partial differential equations (PDEs) and boundary conditions (BCs), respectively, and are minimized to determine the solution.

In this report, the building blocks of a Lagrangian interpolation polynomial are selected as the trial functions  $\psi_i$ . An  $(N-1)th$  order Lagrangian interpolation polynomial  $u_{(N-1)}$  can be considered as a linear combination of  $N$  polynomials of order  $N-1$ , i.e.,  $u_{(N-1)} = \sum_{i=1}^N c_i \psi_i(z)$  where the building blocks are

$$\psi_i(z) = \prod_{\substack{j=1 \\ j \neq i}}^N \frac{(z - z_j)}{(z_i - z_j)}.$$

The coefficient  $c_i$  represents the value of that state at the discretization point  $z_i$  because  $\psi_i(z_j) = \delta_{i,j}$ .

Since the  $\psi_i$  are continuous and differentiable over the entire domain, explicit formulas for differentiation of up to order  $(N - 1)$  can be obtained for all  $z$ . Once the discretization grid is specified, differentiations are matrix-vector operations, i.e.,  $\frac{du}{dz} = A\mathbf{c}$  and  $\frac{d^2u}{dz^2} = B\mathbf{c}$  where the elements of  $a_{ji}$  and  $b_{ji}$  for the differentiation matrices  $A$  and  $B$  are

$$a_{ji} = \frac{d\psi_i(z_j)}{dz} \quad \text{and} \quad b_{ji} = \frac{d^2\psi_i(z_j)}{dz^2}, \quad i, j = 1, 2, \dots, N;$$

and  $\mathbf{c} = [c_1, c_2, \dots, c_N]^T = [u(z_1), u(z_2), \dots, u(z_N)]^T$ . Using Lagrangian building blocks as the global basis trial functions has another advantage. The function value of a Lagrangian polynomial can be evaluated with a recurrence formula as well as its derivatives. In this report, the recurrence formula of Lagrangian polynomial for differentiation matrices are used to facilitate the generation of the matrices [7].

Theoretically, any discretization grid can be used to construct the Lagrangian interpolation polynomial. However, the interpolated solutions between discretization points are accurate only if the individual building blocks behave well between the points. Lagrangian polynomials with a uniform grid will exactly pass through all construction points but will oscillate between points with increasing amplitude near the interval end points. It has been shown [8] that discretization in a quadratic manner towards the ends will suppress the spurious oscillation near the ends. In this report, the discretization positions used (for  $z \in [0, 1]$ ) are the Chebyshev extrema distribution as suggested by Fornberg [8],

$$z_j = \frac{1}{2} \left( \cos \left( \frac{(j-1)\pi}{N-1} \right) + 1 \right), \quad j = N, N-1, \dots, 1.$$

This discretization procedure produces  $4(N - 1)$  nonlinear equations from the modeling PDEs and 8 from the BCs.

Neville's algorithm [9] is used for interpolation. The algorithm is based on rearranging Lagrangian polynomial and noting that any interpolated value of the polynomial, passing through  $z_i, z_{i+1}, \dots, z_{i+m}$ , can be obtained by the values of two lower order polynomials, passing through  $z_i$  to  $z_{i+m-1}$  and  $z_{i+1}$  to  $z_{i+m}$ . A tableau of values thus is established from the zeroth order polynomials, passing through only one point, to the highest order, the interpolation result.

### 3.2 Numerical Continuation

Plasma simulations are well-known to be highly sensitive to small disturbances and so poor initial guesses are unlikely to converge to the solution. A predictor-corrector continuation technique, with an Euler predictor and the Newton corrector step [10], is used in this report to find a converged self-sustained solution corresponding to a low voltage drop, and then to study the solution dependence on the voltage drop.

The simulation was initiated with an external uniform ionization source, i.e., a uniform ionization rate was used in place of the temperature dependent terms  $k_2u_e$ . This is similar to simulation of photoionization. Converged solutions were easily obtained within several iterations. With this set of solution profiles,

the ionization reaction term was gradually modified until the self-sustained solutions was obtained. The homotopy form for the ionization term was used, i.e.,  $(\text{uniform rate}) \times (1 - s) + (k_2 u_e) \times s$  where  $s$  is the continuation parameter. The continuation technique was started at  $s = 0$ , corresponding to the uniform reaction rate, and proceeded to the self-sustained solution of  $s = 1$ . Once a self-sustained solution was reached, the continuation parameter was changed to compute solutions as a function of applied voltage at the powered electrode.

As one method for validating our converged self-sustained solutions, different uniform ionization rates were chosen as initial continuation points. All resulted in the same self-sustained solution. Solutions reported in the next section were found by starting with an ionization rate of  $1 \times 10^{-3}$  and a dimensionless voltage drop of 0.1521. Once a self-sustained solution was reached, the voltage drop was varied as the continuation parameters, for values up to 0.1683 (corresponding to 77.4 volts).

## 4 Results and Discussions

### 4.1 Results for a representative D.C. case

A self-sustained solution for the one-dimensional model with a DC exciting source is shown in figure (1). The number of discretization points used is fifty ( $N = 50$ ). The electric field and currents computed from the basic variables  $V$ ,  $n_e$ ,  $n_+$ , and  $T_e$  are also shown. The results corroborate with those previously reported in the literature [4, 5]. Figure (a) shows the plasma potential, cathode fall region, and the flat bulk phase. The electric field strength is much greater at the powered electrode ( $z = 1$ ) compared to the grounded electrode ( $z = 0$ ); thus ions bombard both electrode surfaces and with greater intensity at the powered electrode. The fact that the electric field passes through zero increases the difficulty of numerical simulation. It suggests that the ‘‘convection’’ changes direction in the center of the reactor, a characteristic difference from the fluid dynamics simulation, and makes some traditional techniques such as upwind finite difference scheme harder to use.

Both sheaths and bulk phases can be seen in the particle number density profiles (figure 1(b)). The numerical continuation results show that if the voltage drop is increased, the difference between the two densities becomes smaller. The most important simulation result is the electron number density in the cathodic sheath. The density inside the sheath is much lower than that of the bulk phase: four order of magnitude according to our simulations. The density in the sheath, however, cannot be treated as zero because the sheath region is the source of the particle generation by electron impact reaction. Zero density here means no reactions. If during the simulation the electron density profile is allowed to oscillate around zero, the adjacent regions of positive and negative ionization rates would cancel each other. To compensate for ‘‘negative’’ reaction values while retaining a significant total charged particle generation rates, the ‘‘positive’’ reaction node values increase, leading to oscillations in the electron temperature curve. Our interpolation

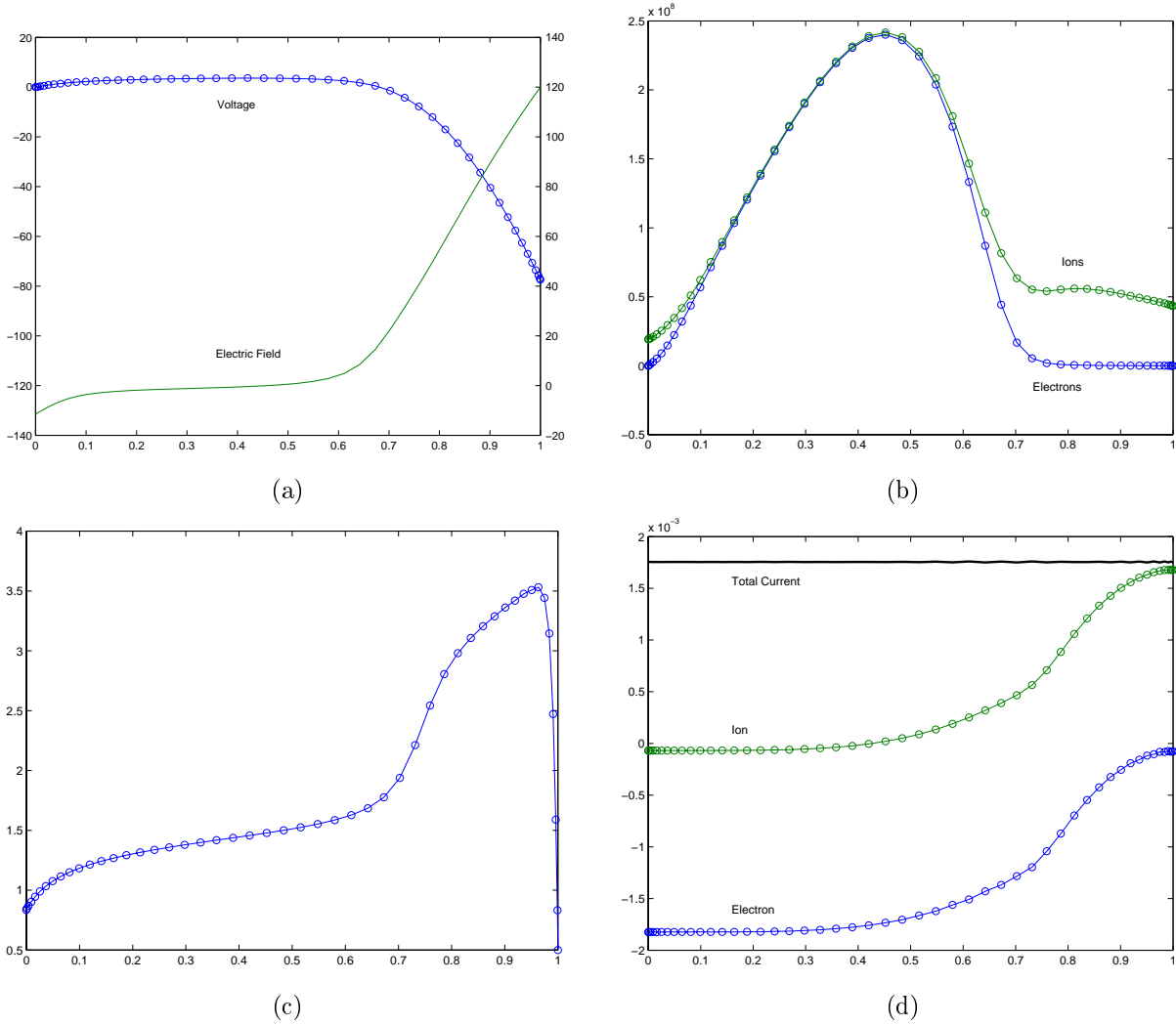


Figure 1: Self-sustained DC solutions. (a) voltage ( $V$  use the left axis) and electric field ( $\frac{V}{cm}$  use the right axis). (b) electron and ion number densities ( $cm^{-3}$ ). (c) electron temperature ( $eV$ ) and (d) electron and ion currents ( $\frac{mA}{cm^2}$ ) versus the dimensionless positions.



curves in figure (2) show no such spurious oscillation.

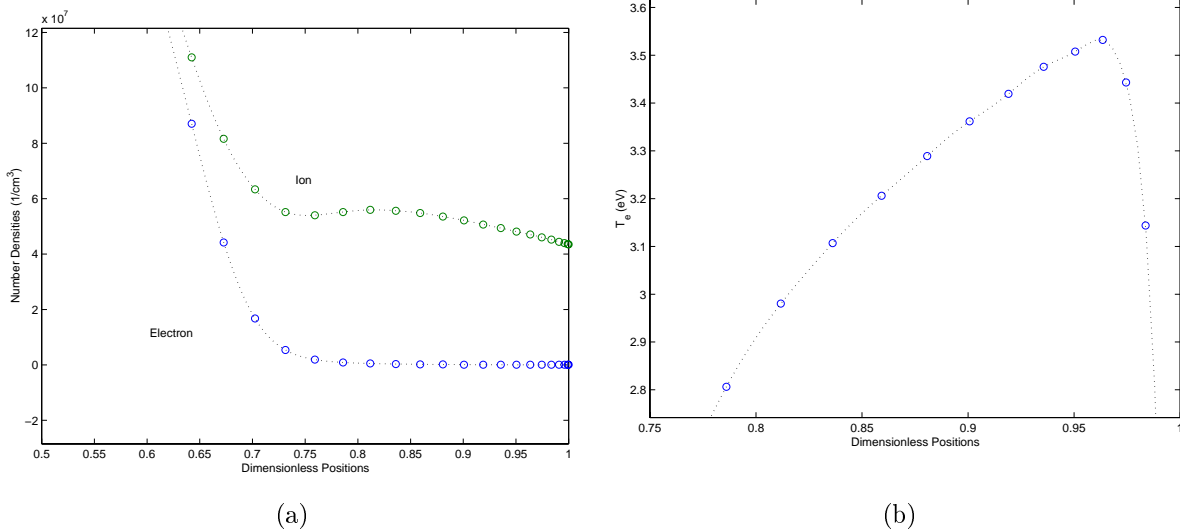


Figure 2: The magnified profiles after interpolation: (a) corresponds to the area near the powered electrode for number densities and (b) is from the electron temperature plot near the powered electrode. The circles represent the solutions right at the collocation points while the dots represent the points obtained after reinterpolation with Lagrangian polynomials.

The mechanism described above is one of several responsible for the numerical stiffness encountered in solving these simulation problems - note that this problem is encountered regardless of the discretization method. The total current shown in figure 1(d) is a constant as it should be in DC case. The electrons are the major current carrier near the grounded electrode while the ions are the one near the powered electrode. The electron current at  $z = 1$  is not equal to zero because of the secondary electron emission boundary condition.

Electron temperature profile (figure 1(c)) also gives the electron energy distribution. Electrons quickly gain energy from the electric field and are accelerated inwards; thus, the temperature increases dramatically near the powered electrode. The curve then quickly dips down due to strong electron cooling by ionization reactions, which are highly endothermic. The bulk phase temperature is rather flat and becomes flatter with increasing voltage drop. The small drop near the grounded electrode is due to the electrons moving against the electric field.

Figure (3) shows the same results with individual terms and associated modeling residuals. According to (a) (the Poisson equation), the electric field gradient faithfully reflects the space charge. (b) shows that the major balancing forces in the electron continuity equation are diffusion and electric drift. The reaction is comparably smaller and may indicate that this discharge is sustained via the secondary electron emissions, i.e., the  $\gamma$  mode discharge. (c) shows that the two major terms are electric drift and ionization. The diffusion

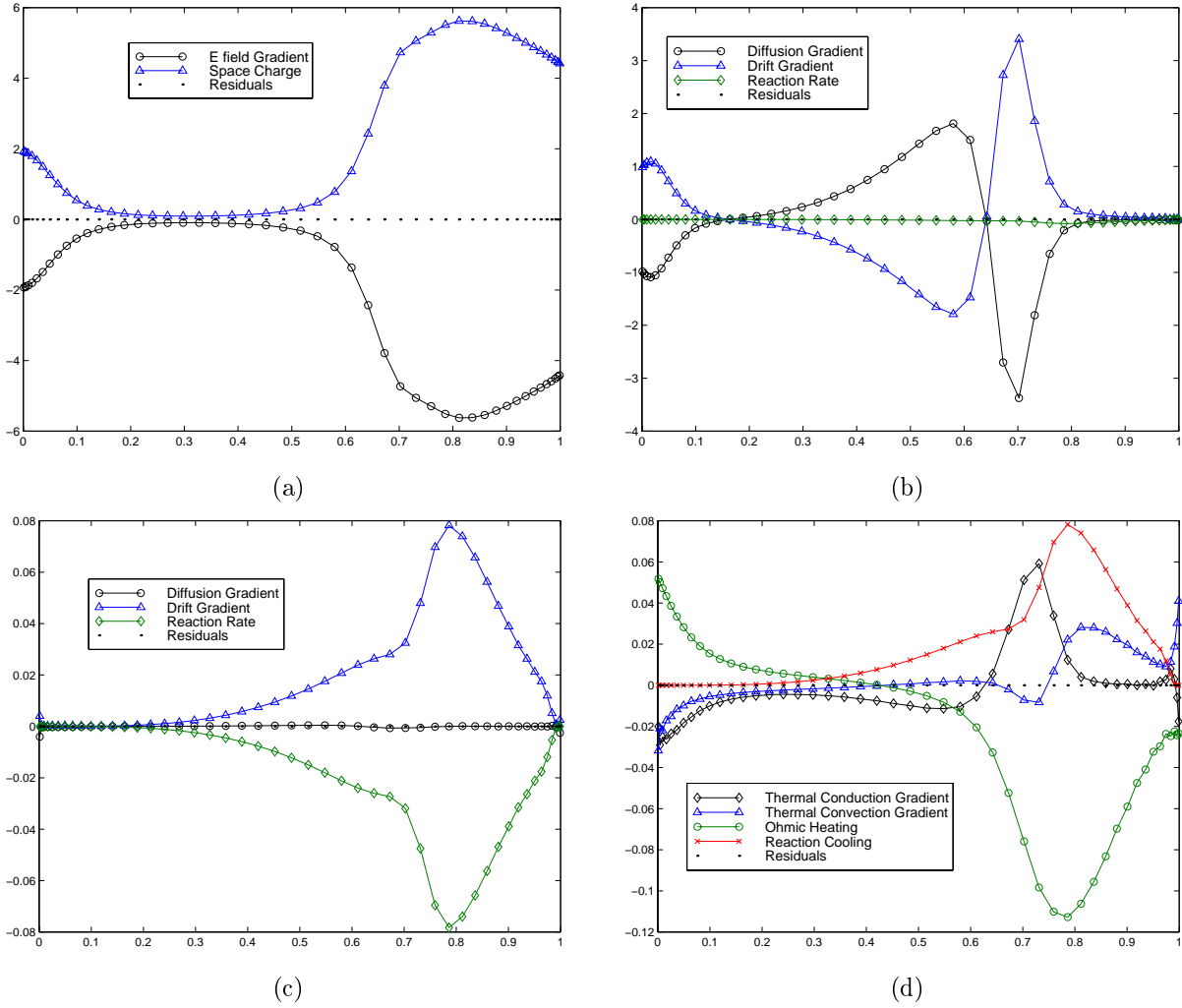


Figure 3: The individual terms in modeling equations with their associated residuals. (a) to (d) are for Poisson equation, electron particle balance, ion particle balance, and electron temperature balance, respectively. The values are in dimensionless form and in terms of dimensionless position.

	At $z = 0$	Residual	At $z = 1$	Residual
$V$	$\Phi = 0$	$9.7047 \times 10^{-28}$	$\Phi = -0.1683$	0
$u_e$	$u_e = 0$	$-1.0768 \times 10^{-27}$	$-\left(\frac{T}{D}\right) \nabla u_e = 1.2924 \times 10^{-8}$ $P_e u_e \nabla \Phi = -4.2510 \times 10^{-4}$ $\left(\frac{\gamma P_+}{D_{e+}}\right) u_+ \nabla \Phi = -4.2509 \times 10^{-4}$	$-2.2630 \times 10^{-19}$
$u_+$	$\nabla u_+ = 0$	$-7.9277 \times 10^{-16}$	$\nabla u_+ = 0$	0
$T$	$\frac{5}{3} \nabla T = 26.1517$ $-\varepsilon_e H_i \nabla \Phi = -26.1517$	$2.3448 \times 10^{-13}$	$T = .5$	0

Table 3: The residuals at the boundary conditions

term is small as expected. Finally, (d) shows a more complicated interaction among four forces. Different terms have different significance locally. The ohmic heating reflects the local electron heating effect. The residuals and the computed boundary conditions are also shown in table (3). As shown in the table, all boundary conditions are completely satisfied.

## 4.2 Temperature Dependent Electron Diffusivity

Plasma fluid models using “diffusion-drift” approximation assume constant diffusivities, which is valid when local acceleration and convection acceleration (inertia) in the momentum balance for each species are negligible (see [3]), and each species temperature is constant. The last assumption is reasonable for heavy species (such as ions) due to their effectiveness of energy exchange with background species, but may not be valid for electrons. Many RF simulations rely on this assumption, while reported DC simulations either take diffusivity temperature dependence explicitly into account [4] or are formulated in terms of the three moment approach and so cannot be directly compared with the diffusion-drift modeling equations. To test the effects of this assumption on the solution behaviors, simulations were performed with equation (1) and were compared to results obtained with a constant  $D_e = 10^6 \frac{cm^2}{sec}$ .

As shown in the figure (4), the temperature dependence of the electron diffusivity has a significant influence on the solutions. For constant  $D_e$ , the number densities are one order smaller (compared with figure 1(b)). The density difference is larger; thus, bulk phase of the voltage profile is not flat. The currents are also smaller than the temperature dependent case. One of the most significant differences, however, is seen in the behavior of the electron temperature as a function of voltage drop. It was found that as the voltage value at  $z = 1$  reaches approximately *80volts*, the temperature at the grounded electrode reaches zero and continues below zero for large voltage drops when a constant  $D_e$  is used.

The observation can be explained by examining the electron energy equation and the solution curves of figure (1) and (4). Near  $z = 0$ , both the ohmic heating ( $-\varepsilon_e \vec{J}_e \cdot \vec{\nabla} \Phi$ ) and reaction cooling ( $k_2 u_e$ ) terms contribute to electron cooling. Because the electron current has a significant magnitude at  $z = 0$  suggests diffusion dominates in this region. Since the electron current, and, hence, electron cooling increases with applied voltage drop, there is no mechanism to prevent  $T_e$  from reaching and passing through zero when  $D_e$  is constant. However, if  $D_e$  is proportional to  $T_e$  (see equation (1)), as the voltage drop increases, the electron diffusion terms become smaller owing to a smaller  $T_e$ , thus alleviating the unrealistic cooling effect.

## 5 Conclusions

A global basis function approach has been used to solve a self-consistent DC glow discharge physics submodel. A continuation technique was used to find the initial self-sustained solution and to study the voltage-drop dependence of the solution. Computed results corroborate with previously published simulations. The

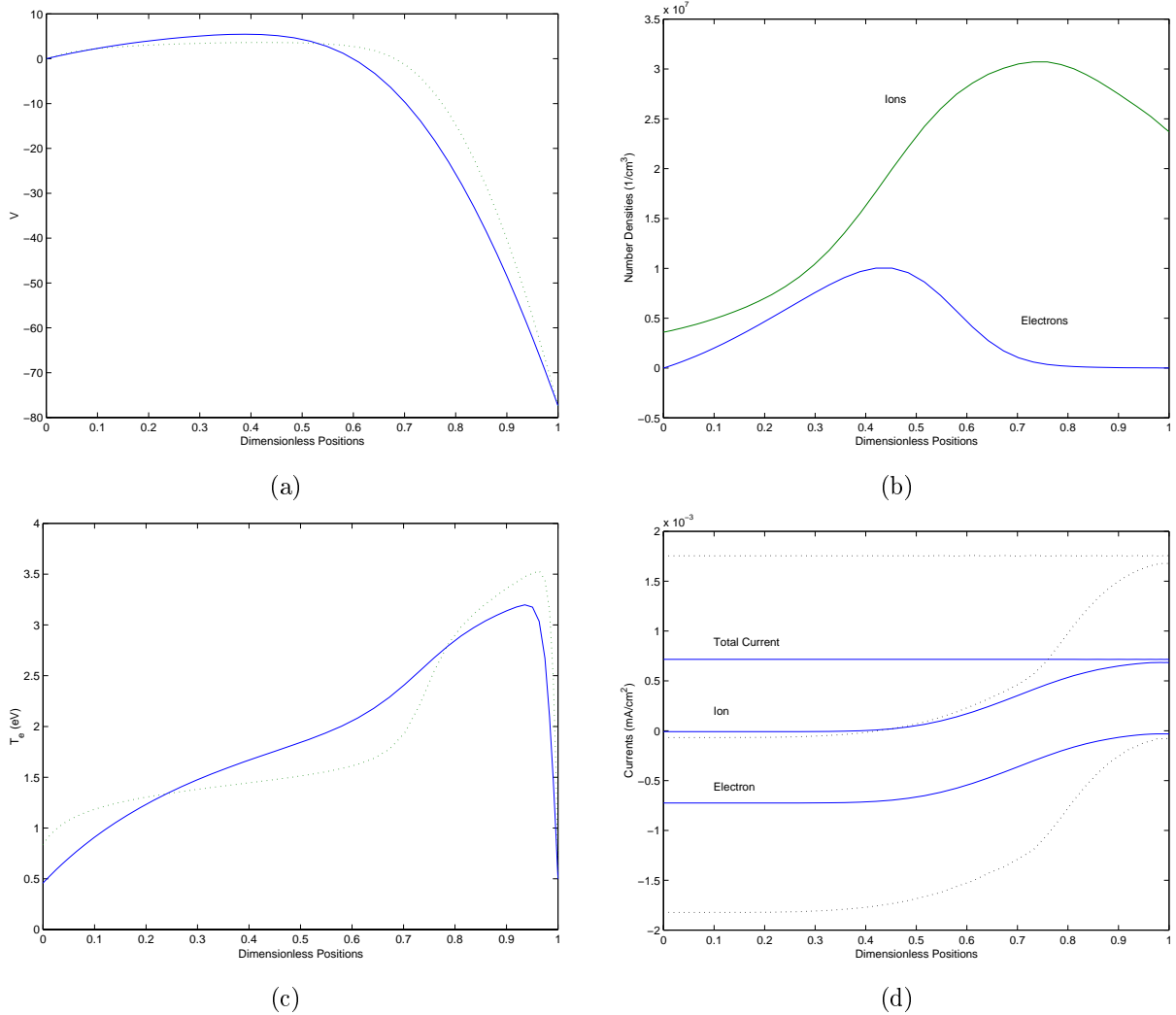


Figure 4: The test results for constant electron diffusivity (solid curves): (a) voltage profile ( $V$ ); (b) the electron and ion densities ( $cm^{-3}$ ); (c) the electron temperature ( $eV$ ); and (d) electron and ion currents ( $\frac{mA}{cm^2}$ ) versus dimensionless position. The dashed curves represent results obtained with electron temperature dependent diffusivity.

residual analysis showed that the modeling equations and the boundary conditions were satisfied accordingly. The interpolation results indicated that the global trial functions behave well between discretization points. The strong influence of the electron temperature on the electron diffusivity was also investigated.

Further studies are in progress for the temperature-dependent electron diffusivity and the global function discretization. The formulation for the diffusivity used in this report may serve as a more accurate but still simple representation than the constant  $D_e$  typically used in RF simulation. The global basis function method on spatial domain provides an alternative approach to discretizing in plasma processing models. Further improvements in simulator performance by generating the differentiation matrices in a fast and numerically more stable manner [11] and by optimization of the trial functions with suitable discretization are in progress.

## References

- [1] Kushner M. J. Advances in plasma equipment modeling. *Solid State Technol.*, page 135, 1996.
- [2] L. E. Kline and M. J. Kushner. Computer simulation of materials processing plasma discharges. *Critical Reviews in Solid State and Materials Sciences*, 16(1):1, 1989.
- [3] M. Meyyappan, editor. *Computational Modeling in Semiconductor Processing*. Artech House, Boston, 1995.
- [4] D. B. Graves and K. F. Jensen. A continuum model of dc and rf discharges. *IEEE Trans. on Plasma Sci.*, 14(2):78, 1986.
- [5] M. Meyyappan and J. P. Kreskovsky. Glow discharge simulation through solutions to the moments of the boltzmann transport equation. *J. Appl. Phys.*, 68(4):1506, 1990.
- [6] G. Gottlieb and S. A. Orszag. *Numerical Analysis of Spectral Methods: Theory and Applications*. Society for Industrial and Applied Mathematics, Philadelphia, 1986.
- [7] R. G. Rice and D. D. Do. *Applied Mathematics and Modeling for Chemical Engineers*. John Wiley & Sons, New York, 1995.
- [8] B. Fornberg. *A Practical Guide to Pseudospectral Methods*. Cambridge University Press, New York, 1996.
- [9] W. H. Press, B. P. Flannery, S. A. Teukolsky, and W. T. Vetterling. *Numerical Recipes in Fortran: The Art of Scientific Computing*. Cambridge Press, New York, 2 edition, 1992.
- [10] E. L. Allgower and K. Georg. Continuation and path following. *Acta Numerica*, page 1, 1993.

- [11] B. D. Welfert. Generation of pseudospectral differentiation matrices i. *SIAM J. Numer. Anal.*, 34(4):1640, 1997.